Korean J. Chem. Eng., 36(11), 1932-1939 (2019)
DOI: 10.1007/s11814-019-0381-0

pISSN: 0256-1115
eISSN: 1975-7220

Enhanced oxygen evolution reaction over glassy carbon electrode modified with NiO_x and Fe_3O_4

Reham Helmy Tammam†, Amany Mohamed Fekry, and Mahmoud Mohamed Saleh

Chemistry Department, Faculty of Science, Cairo University, Giza, Egypt
(*Received 7 March 2019 • accepted 2 September 2019*)

Abstract−Magnetite iron oxide (Fe_3O_4)/nickel oxide (NiO_x) modified glassy carbon (GC) electrode shows enhancement of oxygen evolution reaction (OER) compared to GC electrode modified with single NiO_x or Fe_3O_4 nanoparticles. Many techniques such as linear and cyclic sweep voltammetry, electrochemical impedance spectroscopy (EIS) have been employed. Field-emission scanning electron microscopy (SEM) and energy dispersive X-ray spectroscopy (EDX) are both used for characterization of the electrocatalysts. Effect of loading amount of both NiO_x and Fe_3O_4 and the order of deposition on the OER was studied. A significant improvement of the electrocatalytic properties of the Fe_3O_4/NiO_x binary catalyst modified GC is obtained when NiO_x is electrodeposited on GC/Fe_3O_4 (*i.e.* GC/Fe_3O_4/NiO_x) compared to GC/NiO_x/Fe_3O_4 (where NiO_x is deposited first on the GC then Fe_3O_4). The use of GC/Fe_3O_4/NiO_x (where Fe_3O_4 is deposited first on the GC then NiO_x) for OER in alkaline solution support higher currents and consequently negative shifts of the onset potential of OER compared to that of GC/NiO_x or GC/Fe_3O_4. The obtained electrochemical impedance parameters confirmed the above conclusions. Tafel parameters confirm the superior activity of GC/Fe_3O_4/NiO_x and give insight into the mechanism of the OER on the above electrodes.

Keywords: OER, Fe_3O_4, NiO_x, Catalysis, Nanoparticles

INTRODUCTION

Research in efficient and adequate electrocatalysts for enhanced oxygen evolution reaction (OER) has been under concern in recent years [1-4]. OER is a major part of water splitting [5] with water oxidation:

$2H_2O \rightarrow O_2+4H^++4e^-$	Oxidation (generation of dioxygen)
$4H^++4e^- \rightarrow 2H_2$	Reduction (generation of dihydrogen)
$2H_2O \rightarrow 2H_2+O_2$	Total Reaction

OER electrocatalytic reaction is important owing to its impact on water splitting electrochemistry [6,7] and rechargeable metal-air batteries [8,9]. It is considered to be kinetically sluggish (with respect to hydrogen evolution reaction) and has been researched in pursuit of high efficiency for water electrolyzers. This makes an increase in the demand for pure hydrogen gas as clean fuel cells for the search of efficient, low cost and available anodes for OER. This can decrease the overpotential required for the whole process. Bulk metal oxide electrodes have been known as a preferable candidate for OER in alkaline solutions [10-13]. In this context, single bulk metal oxides of precious metals such as Ir_2O_3 and RuO_2 have been widely studied [14-16]. However, the aforementioned electrodes suffer from high cost and scarcity. Recently, extensive research and practical approaches have been established to offer alternative electrodes of high electrocatalytic activity, stability and low cost. This can be obtained by using alternative catalysts of efficient metal oxides such as Ni and Fe oxides [17-20].

Other OER catalysts depending on existing 3d metals were considered as Ni-containing materials which have special attention due to they have good water oxidation potential and their earth-abundant nature [5]. Mixed bulk metal oxides such as FeO/Co_2O_3 and NiO/FeO have been investigated for such purpose in order to overcome some problems associated with the use of Ir_2O_3 [21-23]. The use of alkaline solution has the advantages of inhibiting metal and metal oxide corrosion, decreasing the overpotential and increasing the solution conductivity.

Nevertheless, the use of metal oxide nanoparticles for OER is still not fully illustrated as in the case of bulk metal and metal oxides [24]. The two reactions take place at the anode and cathode can be written as follows:

$$4OH^- \rightarrow O_2+4e+2H_2O \quad (1)$$

$$4H_2O+4e \rightarrow 2H_2+4OH^- \quad (2)$$

Clear advantages of using metal oxide nanoparticles are the unique electronic and electrocatalytic properties, high surface area and easiness of preparations well. On the other hand, metal oxide nanoparticles have proved unique applications in electrocatalysis [25-27], fuel cells [28-30] and biosensors [31].

Chen et al. [3] examined nickel-based catalysts for methanol oxidation or oxygen evolution reactions (OERs) in basic solution. Nanoparticles were used to get a high surface-to-volume ratio, owing to their greater surface area/weight than larger particles that make them more responsive to some other molecules [2].

Corrigan et al. [32] verified that the catalytic activity for nickel hydroxide was improved when doped with iron which lowered significantly the overpotential for OER [33-36]. For example, Klaus [37]

†To whom correspondence should be addressed.
E-mail: reham_tammam@cu.edu.eg

demonstrated that small amount of iron impurities in the alkaline solution considerably improves the OER activity of $Ni(OH)_2$ electrocatalysts. Such proof suggests the selection of compounds which lead to exhibit synergic effects and enhanced performance. Accordingly, here we account the enhancement of the use of binary catalyst composed of nickel oxide and magnetic iron oxide nanoparticles (Fe_3O_4/NiO_x) (with different loading) modified GC electrode as an anode for OER and the synergic effects upon interaction of NiO_x with Fe_3O_4 in the alkaline solution. The NiO_x is electrodeposited on either bare GC or GC modified with Fe_3O_4 nanoparticles and its behavior towards OER is analyzed. Different electrochemical techniques and surface analysis are used to interpret the performance of such electrodes for OER from the alkaline solutions.

EXPERIMENTAL

1. Materials and Measurements

All the used chemicals were Sigma-Aldrich products. Double distilled water was used. Three-electrode electrochemical cell was used in this study. The working electrode was glassy carbon (GC) (d=3.0 mm) that was mechanical polished with emery paper ranging from 500-1500 and then washed with second distilled water and finally with acetone. Saturated calomel electrode (SCE) and a Pt coil were used as a reference and counter electrodes, respectively. Electrochemical characterization was t by using IM6 Zahner potentiostat, Germany. Fitting the impedance data was carried out using "SIM" program involved with the IM6 package. The amplitude of 10 mV and with a frequency range of 100 kHz to 100 mHz. Scanning electron microscopy (SEM) was done using field emission scanning electron microscope, FE-SEM (FEI, QUANTA FEG 250) near to elemental mapping and EDX Unit (Energy dispersive X-ray analyses), which has accelerating voltage ≈30 kV.

2. Electrode Modification

The GC electrode was modified by magnetite (Fe_3O_4) by casting Fe_3O_4 on either bare GC or GC/NiO_x electrodes. Suspension of Fe_3O_4 (magnetite) in oleic acid (stabilizer) of concentration 12.0 g/L was purchased from Fluka. Certain loading of Fe_3O_4 on the electrode surface was done by controlling the volume of the Fe_3O_4 suspension that is dropped on the electrode by an appropriate micropipette. The electrode is kept to dry in the air before use. Before casting Fe_3O_4 on the GC/NiO_x, the NiO_x is first electrodeposited on the GC.

To modify the GC with NiO_x two steps were done: a-Metallic nickel potentiostatic deposition on the glassy carbon electrode in acetate buffer solution (0.1 M, pH=4.0) which contains 1 mM $Ni(NO_3)_2{\cdot}6H_2O$, and we applied electrolysis at a constant potential (−1 V) for various time durations (2, 4, 10 and 20 minutes); b-Passivation of the obtained metallic Ni particles by cycling the potential between −0.5 and 1 V for 10 cycles at a scan rate of 200 mV/s in 0.1 M phosphate buffer solution (pH=7) [38,39].

RESULTS AND DISCUSSION

1. Characterization of the Electrodes

The modification for GC electrode was done with Fe_3O_4, NiO_x and Fe_3O_4/NiO_x nanoparticles. The latter nanoparticles were introduced to the GC surface in order, *i.e.*, either GC/NiO_x/Fe_3O_4 (NiO_x is electrodeposited first) or GC/Fe_3O_4/NiO_x (Fe_3O_4 is cast first). As discussed in the experimental section, Fe_3O_4 casting on the GC electrode was done by dripping an appropriate volume of the Fe_3O_4 suspension on the GC surface. The used loading levels of Fe_3O_4 are 0.02, 0.085, 0.17 and 0.34 mg cm^{-2} (of the GC electrode area).

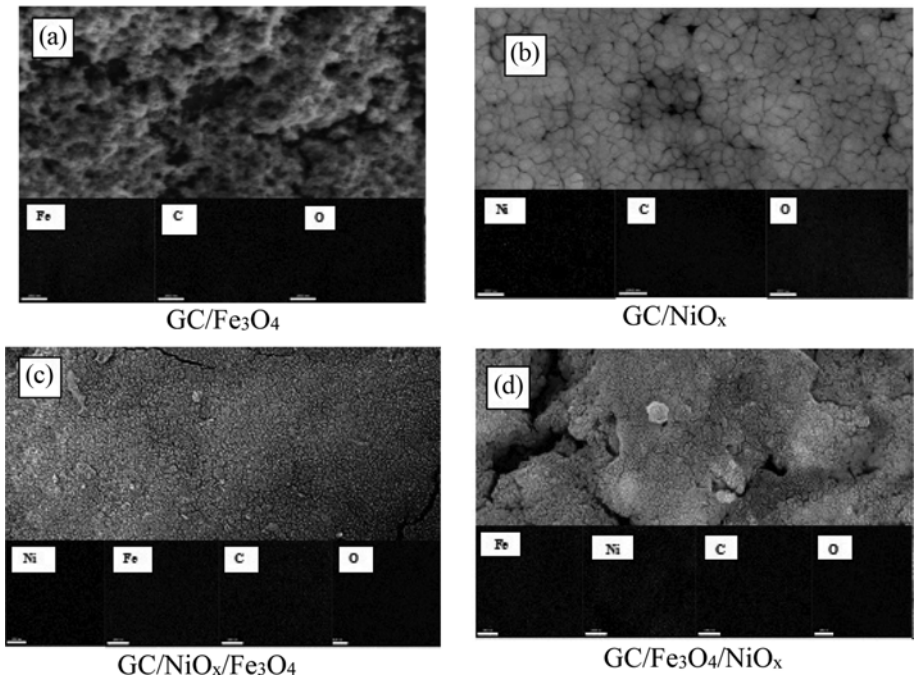

Fig. 1. (a) FE-SEM images and the inset show the elemental mapping of different atoms for GC/Fe_3O_4 (a), GC/NiO_x (b), GC/NiO_x/Fe_3O_4 (c) and GC/Fe_3O_4/NiO_x (d).

To calculate the loading level of Ni during electrodeposition, (I–t) transient current-time relations were done at different conditions both in a solution containing Ni ions and in Ni ions-free solution. Subtracting the total current (I_t=I_{Ni}+I_H) from the current in blank solution (Ni ion-free solution), I_H gives the value of current for nickel electrodeposition, I_{Ni}. The nickel currents at different time periods were used for determination of the charge passing through the whole electrodeposition process, Q_{Ni}. Using the last values we can calculate the nickel loading levels by using Faraday's law. The calculated values of the NiO_x loading levels on the GC electrode are 0.0197, 0.0504, 0.207 and 0.430 mg cm^{-2}. The equivalent loadings on the GC/Fe_3O_4 electrode are 0.0294, 0.075, 0.240 and 0.529 mg cm^{-2} which correspond to the same time intervals of 2, 4, 10 and 20 min, respectively.

Fig. 1(a) presents SEM images for GC/Fe_3O_4 (a), GC/NiO_x (b), GC/NiO_x/Fe_3O_4 (c) and GC/Fe_3O_4/NiO_x (d). Fig. 1(a) shows that Fe_3O_4 nanoparticles (image A) are semispherical in shape with an average particle size ≈40 nm and uniformly cover the surface of GC. For the NiO_x (image B), the nanoparticles show semispherical shape with an average diameter of ~90 nm (larger size than Fe_3O_4) with reasonable uniform distribution on the surface. In images (C), we can see that NiO_x/Fe_3O_4 (NiO_x deposited first) shows similar features with the image A (i.e., Fe_3O_4) where Fe_3O_4 may cover most of NiO_x surface. Image D (Fe_3O_4/NiO_x), where Fe_3O_4 eas cast first, demonstrates NiO_x particles of larger size than Fe_3O_4 on the top of the latter. The EDX charts (shown in supplementary materials S1) for Fe_3O_4 (chart a) show typical peaks of C (GC), peaks of O and Fe as the atomic structure of the Fe_3O_4. In the EDX charts c and d (shown in supplementary materials S1), related to GC/NiO_x/Fe_3O_4 and GC/Fe_3O_4/NiO_x, respectively, reveal characteristics peaks of Fe and Ni. We may conclude that both elements (Ni and Fe (and hence oxides, Fe_3O_4 and NiO_x) are exposed to solutions and yet no complete coverage of one component (oxide) is obtained by the other component (oxide). However, in chart c (Fe_3O_4/NiO_x), the Ni peaks are more pronounced than that in chart b (NiO_x/Fe_3O_4). In the latter, Fe_3O_4 may have covered the NiO_x surface. This may give rise to possible synergism where the two metal oxides are exposed to the solution and hence participate in the OER. The distributions of the different elements for each electrode are presented in the inset of Fig. 1(a). For all studied electrodes uniform distribution of the elements along the whole electrode surfaces, which enhances the chance to increase its electrochemical active surface area and in turn enhances their role in OER.

Characteristics CVs for the different electrodes were measured in 0.5 M NaOH at 100 mV s^{-1} as shown in Fig. 2. As can be seen, GC electrode (a) does not reveal any features at this potential range. For the GC/Fe_3O_4 (b), a broad peak starts from E=0.5 V, which is corresponding to the following reaction [40,41]:

$$Fe_3O_4+16OH^- \rightarrow 3FeO_4^{2-}+8H_2O+10e^- \quad (3)$$

where Fe_3O_4 is converted to ferrate ion (FeO_4^{2-}) in the present alkaline medium. For the three electrodes, GC/NiO_x (c), GC/NiO_x/Fe_3O_4 (d), and GC/Fe_3O_4/NiO_x (e), their CVs reveal a couple of peaks corresponding to NiOOH/$Ni(OH)_2$ redox pair in the potential range of 0.3-0.5 V. However, the values of peak current (I_p) and onset potential depend mainly on the electrode type. For instance, Fe_3O_4/NiO_x

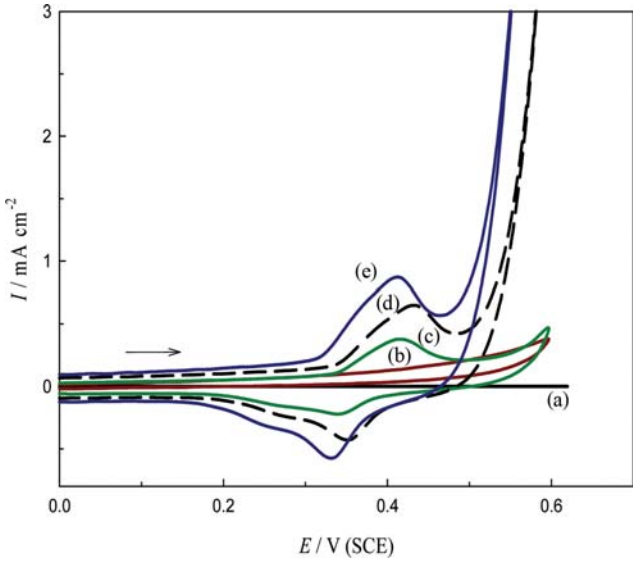

Fig. 2. CV for the different electrodes in 0.5 M NaOH at 100 mV s^{-1} scan rate: (a) GC, (b) GC/Fe_3O_4, (c) GC/NiO_x, (d) GC/NiO_x/Fe_3O_4 and (e) GC/Fe_3O_4/NiO_x (NiO_x loading=0.207 mg cm^{-2} in (c) and (d) and 0.240 mg cm^{-2} in (e). Fe_3O_4 Loading is 0.17 mg cm^{-2}.

shows the highest value of I_p and bearing negative shift in the onset potential for the redox couple. One way to explain the high values of peak currents (both in the anodic and the cathodic sweeps) is to consider the oxidation power of the ferrate ion, FeO_4^{2-} which can convert $Ni(OH)_2$ to NiOOH and enrich the nickel oxide matrix with a high concentration of the Ni(III)ions.

Inspection of the CV obtained at the GC/Fe_3O_4/NiO_x electrode (curve e) gives some features. The peak currents of both Ni(II)/Ni(III) redox couple both in the anodic and cathodic scans at the GC/Fe_3O_4/NiO_x are the highest among the used electrodes. For instance, I_p is doubled compared with NiO_x/GC (curve c). The loading extents for NiO_x on both GC (GC/NiO_x) and on Fe_3O_4 (GC/Fe_3O_4/NiO_x) are 0.207 and 0.240 mg cm^{-2}, respectively. This difference in loading cannot count for the large increase in the peak current of the $Ni(OH)_2$/NiOOH transformation shown in Fig. 2. One can attribute the current peak enhancement of the couple Ni(II)/Ni(III) to the increase of the active species concentration (Ni(III) and/or Ni(II)) in the mixed oxide matrix (*i.e.*, Fe_3O_4/NiO_x).

The surface concentration is the concentration of the immobilized electroactive containing-nickel species at the electrode surface (Γ). The value of Γ can be expected from the charge used during the redox transformation of Ni(II)/Ni(III), (i.e., Γ=Q/nFA), where Q is the charge (Q can be calculated from the CVs shown in Fig. 2), n is the number of electrons, F is the Faraday constant (96,500 C mol^{-1}) and A is working electrode surface area. The values of Γ were found to be 5.3×10^{-5}, 7.2×10^{-5} and 9.8×10^{-5} mmol cm^{-2} for GC/NiO_x, GC/NiO_x/Fe_3O_4, and GC/Fe_3O_4/NiO_x, respectively. These values of Γ confirm the above-mentioned conclusion. The generation of the ferrate ion in the oxide matrix causes the oxidation of the $Ni(OH)_2$ and accordingly, it converts some of the Ni^{2+} to Ni^{3+} and increases the conductivity of the oxide matrix according to

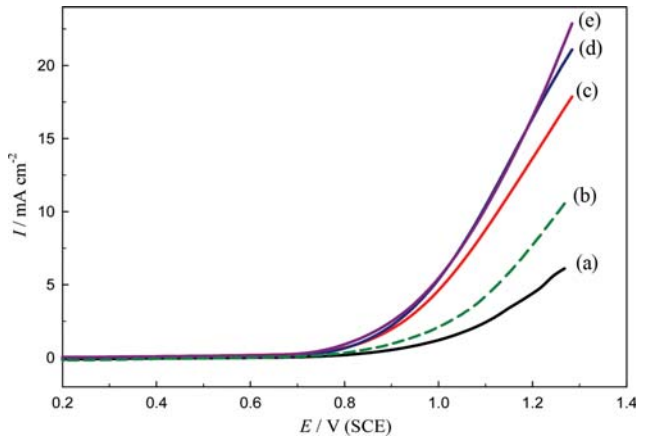

Fig. 3. LSV for OER in 0.5 M NaOH on GC/Fe_3O_4: (a) GC, and GC/Fe_3O_4 of different loadings: (a) GC, (b) 0.02, (c) 0.085, (d) 0.17 and (e) 0.34 mg cm^{-2}, at a scan rate of 10 mV s^{-1}.

the reaction:

$$Fe(IV)+Ni(II)\rightarrow Ni(III)+Fe(III) \quad (4)$$

One more feature regarding the enrichment in the Ni(II)/Ni(III) couple is the more negative shift in the onset potential and peak potential of the Ni(II)/Ni(III) redox couple GC/Fe_3O_4/NiO_x electrode as compared with the NiO_x/GC electrode (curve c), confirming the enhancement of the kinetics of Ni(II)/Ni(III) redox species. Also, the order of deposition of NiO_x is important since GC/Fe_3O_4/NiO_x offers better exposure of the NiO_x to the electrolyte than that offered by GC/NiO_x/Fe_3O_4.

2. Oxygen Evolution Reaction (OER)

The OER was studied by making linear sweep voltammetry (LSV) in the range of 0.2 V to an upper potential in the OER range in 0.5 M NaOH. Optimization of the electrocatalysts loading is significant in the electrochemical systems. Fig. 3 illustrates LSV of GC/Fe_3O_4 electrode at different Fe_3O_4 loadings on the GC. These loadings are 0.02, 0.085, 0.17 and 0.34 mg cm^{-2}. By Comparing to bare GC (curve a), the GC/Fe_3O_4 shows a great enhancement with values of the current depend on the loading level. Also, there is a less positive shift in the onset potential, E_{onset} of the OER. For example, loading of 0.085 mg cm^{-2} of Fe_3O_4 (curve c) causes a 150 mV in the onset potential and five-times increase in the current of the OER at 1.2 V. As can be seen, there is no significant enhancement of the OER observed at loading of Fe_3O_4 higher than the range of 0.17 mg cm^{-2}. That is, a loading range of ~0.17 mg cm^{-2} is proper for OER at the current experimental conditions. It is well documented in the literature [42-44] that iron oxide coated electrodes enhance OER from the alkaline solution.

Fig. 4(A) represents LSV responses for OER on GC/Fe_3O_4/NiO_x electrode in 0.5 M NaOH. The electrode was prepared by first casting Fe_3O_4 on the GC electrode at its proper loading as concluded from Fig. 3, *i.e.*, 0.17 mg cm^{-2}. In Fig. 4, an attempt to optimize the NiO_x loading at the present experimental conditions is achieved by electrodeposition of NiO_x using different time periods. The NiO_x loading levels used in Fig. 4 are 0.0294, 0.075, 0.240 and 0.529 mg cm^{-2} corresponding to deposition time, 2, 4, 10 and 20 min, respectively. Fig. 4(B) shows the change of the current value of the OER at E=0.8, 1.0 and 1.2 V at different NiO_x loadings on the GC/Fe_3O_4 (where loading of Fe_3O_4 is kept constant at 0.17 mg cm^{-2}). The figure shows a considerable increase of the OER currents (at definite potential) with the NiO_x loading level. In Fig. 4(B), the change of the OER current density at different potential is presented. The current (rate) increases with the loading of NiO_x before it reaches a constant value depending on the potential, E. High potentials support higher currents with higher sensitivity to the loading level. However, no significant difference in the currents obtained at loading level higher than 0.240 mg cm^{-2} at all potentials. This may point to the nature of the surface catalytic of the OER process and yet not all the NiO_x matrix is active for the OER.

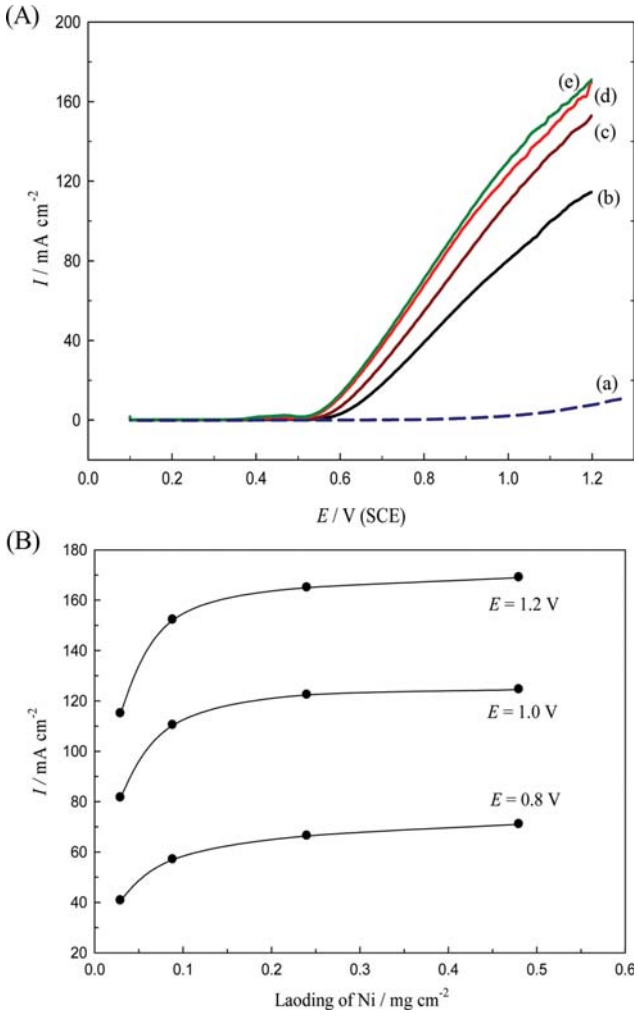

Fig. 4. (A) LSV for OER in 0.5 M NaOH on GC/Fe_3O_4/NiO_x of different loadings of NiO_x: (a) 0, (b) 0.029, (c) 0.075, (d) 0.24 and (e) 0.529 mg cm^{-2}, at a scan rate of 10 mV s^{-1}. (B) Variation of the current of OER on GC/Fe_3O_4/NiO_x with the NiO_x loading level (Fe_3O_4 loading is fixed at 0.17 mg cm^{-2}).

Fig. 5 shows LSV responses for OER on GC (a), GC/Fe_3O_4 (b), GC/NiO_x (c), GC/NiO_x/Fe_3O_4 (d) and GC/Fe_3O_4/NiO_x (e). The loading of NiO_x is 0.240 mg cm^{-2} and for Fe_3O_4 is 0.17 mg cm^{-2}. Note that the difference in the case (b) and case (d) is that the Fe_3O_4 was cast (with the same amount of loading) on GC and on GC/NiO_x,

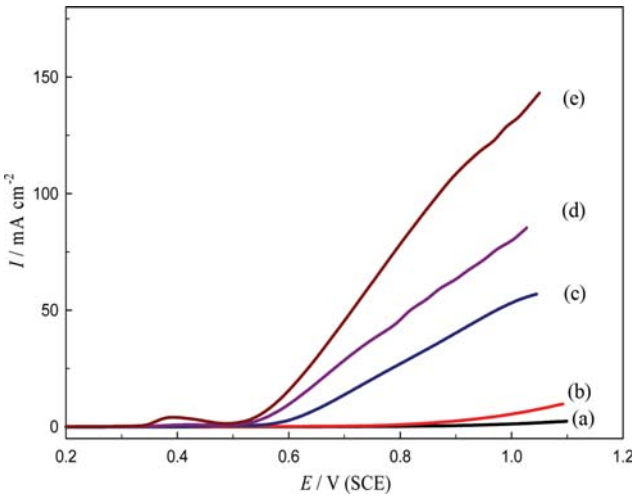

Fig. 5. LSV responses for OER for different electrodes in 0.5 M NaOH: (a) GC, (b) GC/Fe_3O_4, (c) GC/NiO_x, (d) GC/NiO_x/Fe_3O_4 and (e) GC/Fe_3O_4/NiO_x (loading of NiO_x=0.207 mg cm^{-2} in (c) and (d) and 0.240 mg cm^{-2} in (e). Fe_3O_4 loading is fixed at 0.17 mg cm^{-2}.

respectively. The figure shows clearly variant activities of the electrodes towards OER. Although GC/Fe_3O_4 reveals higher currents and hence superior catalytic activity for OER compared with bare GC electrode (see Fig. 3(c)), it is much less active than the other electrodes. LSV for GC/NiO_x was also studied (see the supplementary materials Fig. S2). The results show that there is an increase in the value of OER current as the nickel loading increase, but still less than both electrodes which are GC/NiO_x/Fe_3O_4 and GC/Fe_3O_4/NiO_x electrodes.

A remarkable enhancement of the OER was obtained when Fe_3O_4 was cast on GC/NiO_x (curve d, GC/NiO_x/Fe_3O_4) when compared with that cast on bare GC (curve b, GC/Fe_3O_4). Also, when Fe_3O_4 is cast on top of the GC/NiO_x, it supports higher currents for the OER than that supported by GC/Fe_3O_4 or GC/NiO_x. For instance, at a potential E=1.0 V, the current increases from 3 mA cm^{-2} at GC/Fe_3O_4 to 75 mA cm^{-2} at GC/NiO_x/Fe_3O_4 electrode. That is, the GC/NiO_x/Fe_3O_4 (NiO_x is deposited first) supports greater currents for OER, which is higher by ~12 and 1.5-times compared to GC/Fe_3O_4 and GC/NiO_x, respectively at E=1.0 V.

When NiO_x is electrodeposited on GC/Fe_3O_4 (*i.e.,* GC/ Fe_3O_4/NiO_x, curve e), it supports higher currents than that of GC/NiO_x/Fe_3O_4 (and consequently higher than that of GC/NiO_x). One can conclude that the order of deposition of NiO_x and Fe_3O_4 is a crucial factor. Table 1 shows the current density of OER at different potentials at two loadings of NiO_x for the different electrodes (0.029 and 0.240 mg cm^{-2}). The potentials are 0.6, 0.8 and 1.0 V, which represent low, intermediate and high potentials (polarization). The same trends shown in Fig. 5 can be derived from Table 1. The largest difference and enhancement was obtained at E=1.0, which is of practical importance. Note that mixed metal oxides are known for enhancement to OER [45,46]. However, in the present work, different orders (layer atop of layer) of loading the oxide nanoparticles were used. This was explained in the light of the synergism between Fe_3O_4 and NiO_x and also from the fact that NiO_x may be electrodeposited on GC/Fe_3O_4 with a different electrocatalytic active phase compared with that electrodeposited on the GC [47,48]. Furthermore, the enhanced OER activity of the oxide nanoparticles originated due to the synergic effects resultant from the interaction of Fe_3O_4 with NiO_x, since the isolated materials, particularly Fe_3O_4 or NiO_x, have much lower activity than the respective binary oxide nanoparticles [49]. The synergistic effect between Ni and Fe has received extensive attention since researchers realize that even a few amounts of iron incorporation can greatly improve the turnover frequency of Ni-based materials and then significantly enhance their OER activity [50]. Even though the exact mechanism for the synergistic effect is still under discussion, the strategy in different material systems has been widely published [51-54].

Our study gives a high current density reaching about 131.4 mA cm^{-2} compared to others in the previous study, which is 111 mA cm^{-2} as obtained by Yoon et al. [30] and 10 mA cm^{-2} as found by Gonçalves et al. [49] who used alpha-Ni$(OH)_2$- FeOCPc@rGO composite for OER.

To explain the significant enhancement in the OER on the GC/Fe_3O_4/NiO_x electrode, Nyquist and Bode diagrams were measured at similar conditions taken in Fig. 5. Fig. 6(a) and (b) show Nyquist plot and Bode diagram for the different electrodes at E=0.7 V. The Nyquist plots illustrate a semicircle with a diameter dependent on the electrode. The diameter decreases in the following order: GC>GC/Fe_3O_4>GC/NiO_x>GC/NiO_x/Fe_3O_4>GC/Fe_3O_4/NiO_x. Analysis for EIS data was done by fitting to a related equivalent circuit as shown in Fig. 7. R_s, Q_{dl} and R_{ct} which correspond to the solution resistance, a constant phase element equivalent to the double-layer capacitance and the charge transfer resistance associated with the OER, respectively [55]. Analysis of the EIS data was done to extract important electrochemical parameters.

To show an acceptable impedance simulation of the data in Fig.

Table 1. The effect of NiO_x loading (0.029 and 0.24 mg cm^{-2}) or Fe_3O_4 loading at 0.17 mg cm^{-2} with current density, I as a function of potential, E and the onset potential of OER, E_{onset}

E/V	GC		GC/Fe_3O_4		GC/NiO_x		GC/NiO_x/Fe_3O_4		GC/Fe_3O_4/NiO_x	
	0.029 mg cm^{-2}	0.24 mg cm^{-2}	0.029 mg cm^{-2}	0.24 mg cm^{-2}	0.029 mg cm^{-2}	0.24 mg cm^{-2}	0.029 mg cm^{-2}	0.24 mg cm^{-2}	0.029 mg cm^{-2}	0.24 mg cm^{-2}
0.6	1.1	1.1	0.91	1.1	1.0	3.2	3.76	10.2	10.75	15.9
0.8	1.2	1.2	1.5	1.5	9.85	26.9	15.7	45.0	53.25	78.5
1.0	1.3	1.3	6.7	6.7	21.5	53.4	37.5	80.7	101.5	131.4
E_{onset}/V	1.0	1.0	0.81	0.81	0.599	0.561	0.580	0.510	0.510	0.452

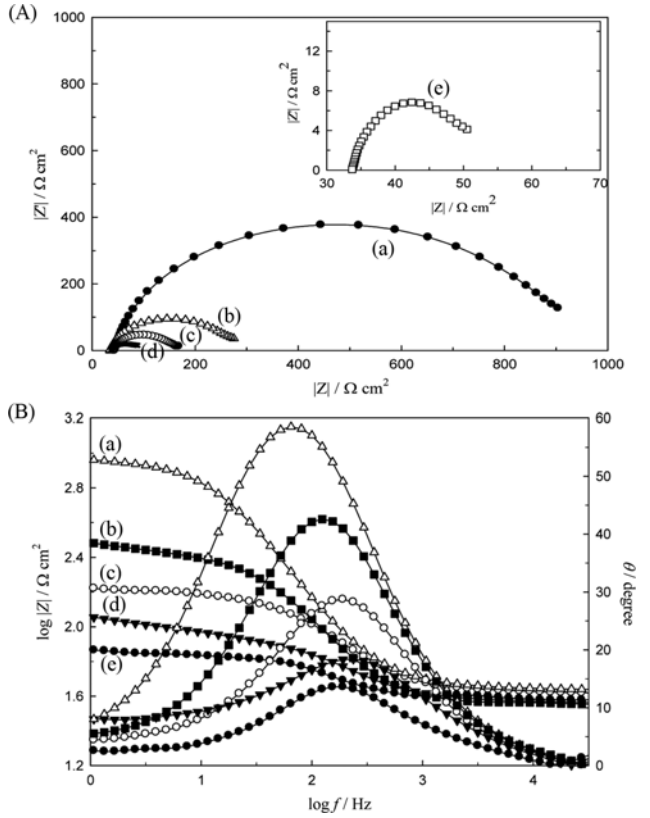

Fig. 6. ((A) and (B)) Nyquist and Bode Plots for the different electrodes in 0.5 M NaOH at 0.7 V: (a) GC, (b) GC/Fe_3O_4, (c) GC/NiO_x, (d) GC/NiO_x/Fe_3O_4 and (e) GC/Fe_3O_4/NiO_x (NiO_x loading=0.207 mg cm^{-2} in (c) and (d) and 0.240 mg cm^{-2} in (e). Fe_3O_4 Loading is 0.17 mg cm^{-2}.

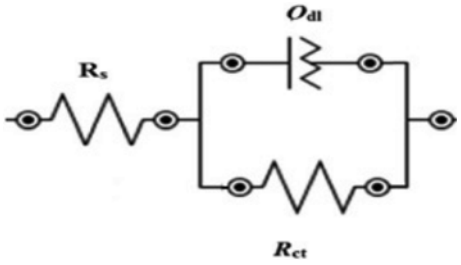

Fig. 7. Equivalent fitting circuit used for EIS figures (Fig. 6).

Table 2. Electrochemical impedance fitting parameters for the different electrodes at a loading of NiO_x (0.24 mg cm^{-2}) and Fe_3O_4 (0.17 mg cm^{-2})

Electrode	R_{ct}/Ω cm^2	Q_{dl}/μF cm^{-2}	α	R_s/Ω cm^2
GC	1000	8	0.67	40
GC/Fe_3O_4	434	18	0.72	37
GC/NiO_x	240	22	0.67	43
GC/NiO_x/Fe_3O_4	158	27	0.74	38
GC/Fe_3O_4/NiO_x	97	34	0.60	38

6(a) and (b), we replaced the capacitor (C) with a constant phase element (CPE) in the proposed equivalent circuit. CPE is referred to as Q_{dl} in Table 2 which was due to the microscopic roughness which leads to an inhomogeneous distribution for the capacitance of the double layer [56]. The impedance of a constant phase element (Z_{CPE}) is known as $Z_{CPE}=[Q_{dl}(j\omega)^{\alpha}]^{-1}$, where $j=(-1)^{1/2}$, $-1\leq\alpha\leq1$, ω (angular frequency in rad/s) $\omega=2\pi f$ is the, f is the frequency measured in Hz=s^{-1}, α is an empirical exponent fitting parameter which varies between 1 and 0 and is used to account for the deviation from the ideal capacitive behavior due to many factors [57-59]. In our work, an acceptable agreement between theoretical and experimental data was found (average error of 2.5%). The expected impedance parameters are given in Table 2. The α values for the different electrodes ranged between 0.60 and 0.72, which confirms that the oxide electrodes do not act as a perfect capacitor. The results demonstrate that the phase angle (Fig. 6(b)) has values below 90° which confirms the non-ideality of the capacitive behavior for the studied oxides. At the potential (E= 0.7 V), the OER is under charge-transfer mechanism and so R_{ct} can be gained from the EIS figures. The value of R_{ct} has the order: GC>GC/Fe_3O_4>GC/NiO_x>GC/NiO_x/Fe_3O_4>GC/Fe_3O_4/NiO_x. This confirms that OER on the GC/Fe_3O_4/NiO_x is facilitated compared to the other electrodes.

An attempt to interpret the enhancement of the OER on the GC/Fe_3O_4/NiO_x is introduced by considering the CVs for different electrodes in a narrow potential range. The latter is a potential range between 0.1-0.55 V and in which a redox couple transformation of Ni(II)/Ni(III) (i.e., $Ni(OH)_2\leftrightarrow NiOOH+1e$) takes place (see Fig. 2). The other electrodes (GC/NiO_x, GC/NiO_x/Fe_3O_4 and GC/Fe_3O_4/NiO_x) show redox peaks for the couple Ni(II)/Ni(III) with current peak value depends on the electrode type. The order of the peak current of the Ni(II)/Ni(III) transform is GC/Fe_3O_4/NiO_x>GC/NiO_x/Fe_3O_4>GC/NiO_x (see Fig. 2). The presence of the Fe_3O_4 in the internal layer enhances the redox couple transformation more than its presence in the external layer. Since the increase in I_p of the Ni(II)/Ni(III) transformation coincide with the enhancement in the OER (obtained in Fig. 2), one may correlate the two trends. Yet, we may consider the role of the NiOOH species in the OER mechanism and its catalytic role that facilitate the OER.

It is well documented in the literature that Fe_3O_4 (magnetite) is anodically converted to FeO_4^{2-} (ferrate ion) in alkaline electrolyte. The oxidizing power of FeO_4^{2-} ion applied for the oxidation of organic and inorganic species [60,61]. In this context, the ferrate ion may oxidize $Ni(OH)_2$ species to NiOOH at anodic potential range (0.3-0.6 V) according to the following proposed equations:

$$Fe_3O_4\rightarrow FeO_4^{2-} \quad (5)$$

$$Ni(II)+FeO_4^{2-}\rightarrow Ni(III)+Fe(II+III) \quad (6)$$

The enhancement of the NiO_x matrix with Ni^{3+} species causes an increase in the conductivity of the matrix (NiO_x) and hence enhancement in the OER on the GC/Fe_3O_4/NiO_x electrode.

Fig. 8 shows Tafel plots for OER on GC/NiO_x (a), GC/NiO_x/Fe_3O_4 (b) and GC/Fe_3O_4/NiO_x (c) in 0.5 NaOH. The potential was corrected to the ohmic drop (IR) using data extracted from the EIS data. The figure reveals two straight lines with different slopes. A slope of 55 mV dec^{-1} (±5 mV) is obtained at a low potential range and a slope of 130 mV dec^{-1} (±5 mV dec^{-1}) at high potential range

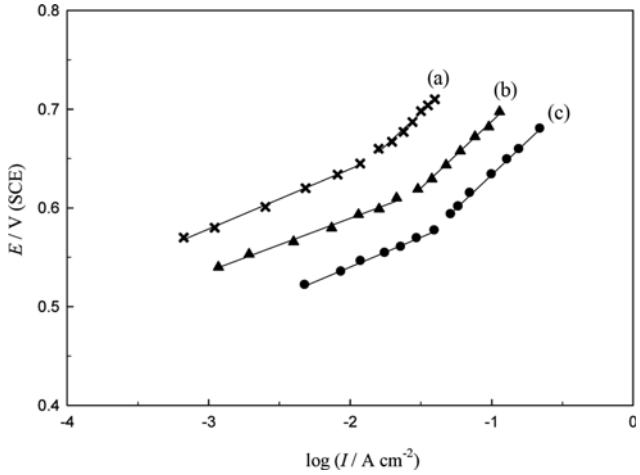

Fig. 8. Tafel plots for OER on (a) GC/NiO_x, (b) GC/NiO_x/Fe_3O_4 and (c) GC/Fe_3O_4/NiO_x, at scan rate of 10 mV s^{-1}.

Table 3. Tafel slopes (mV dec^{-1}) for OER on the different electrodes at low and high potentials

Electrode	GC/NiO_x	GC/ NiO_x/Fe_3O_4	GC/Fe_3O_4/ NiO_x
Low potential	54	61	66
High potential	133	134	135

(see Table 3). The above result of Two Tafel slopes is documented in the literature [62,63].

It has been demonstrated in the literature that a considerable rate of the OER from alkaline solutions starts at potentials higher than $Ni(OH)_2$/Ni(OOH) peak potential [63,64]. As shown in Fig. 5, the uncoated GC (a) and GC/Fe_3O_4 (b) electrodes offer non-significant rates of the OER, while on the other electrodes GC/NiO_x (c) GC/NiO_x/Fe_3O_4 (d) and GC/Fe_3O_4/NiO_x (e), the $Ni(OH)_2$/Ni(OOH) anodic peak of is obviously preceding the E_{onset} of the OER. It may be concluded that OER does not start at the oxyhydroxide (NiOOH) sites and yet another active phase is formed from the oxyhydroxide at higher potentials. That active species can mediate and support the high current obtained for the OER. This conclusion is in agreement with that found in the literature [62-65] where the formation of NiO_2 (as reactive species) mediates the OER in alkaline solutions at NiOOH modified electrodes. A recently proposed mechanism [62-64] for OER at similar conditions can be summarized as follows:

$$NiOOH+OH^- \rightarrow NiO(OH)_2+e \quad E=1.434\ V\ (RHE) \quad (7)$$

$$NiO(OH)_2+OH^- \rightarrow NiO(OOH)+H_2O+e \quad (8)$$

$$NiO(OOH)+OH^- \rightarrow NiOO_2+H_2O+e \quad (9)$$

$$NiOO_2+OH^- \rightarrow NiOOH+O_2+e \quad (10)$$

As can be seen from the above-mentioned mechanism, it involves the formation of adsorbed peroxide intermediate ($NiOO_2$).

The above mechanism is in agreement with the data obtained in Fig. 5 (and also with Tafel slopes obtained in Fig. 8). For instance, the E_{onset} for OER obtained from Fig. 5 is ~1.47 V (RHE), which is consistent with the standard potential of Eq. (7). The other remark here is that the average Tafel slope at low potentials regions on the three electrodes is ~58 mV dec^{-1} (Table 3), which suggests the first step (Eq. (7)) as a pseudo-equilibrium step and the second step (Eq. (8)) is a rate-determining step (total of 2 e^-) . At high potential, the average Tafel slope increases to ~130 mV dec^{-1}, a value which favors the suggestion that the first step (Eq. (7)) is the rate-determining step (1 e^-). Generally, we conclude that the electrocatalytic activity of NiOOH depends on its ability to transfer electrons to the conducting substrates.

CONCLUSIONS

The study evaluated the use of magnetite iron oxide/nickel oxide (GC/Fe_3O_4/NiO_x) binary nanoparticles modified GC electrode for OER from alkaline solution at different loadings. The Fe_3O_4 was cast on different substrates: one on bare GC and the other on GC/NiO_x. On the other hand, NiO_x was electrodeposited on either bare GC or GC/Fe_3O_4. Significant enhancement of the OER was obtained when NiO_x was electrodeposited on GC/Fe_3O_4 (*i.e.*, GC/Fe_3O_4/NiO_x) compared to either of GC/NiO_x/Fe_3O_4 (NiO_x is deposited first), GC/NiO_x or GC/Fe_3O_4. EIS data confirmed the above conclusions. Optimization of the loading levels of both Fe_3O_4 and NiO_x was possible under the prevailed experimental conditions. Analysis of the polarization data through the plotting of Tafel plots revealed a suggestion of the mechanism for the OER on the different electrodes.

SUPPORTING INFORMATION

Additional information as noted in the text. This information is available via the Internet at http://www.springer.com/chemistry/journal/11814.

REFERENCES

1. X. Liu, Z. Sun, S. Cui and P. Du, *Electrochim. Acta*, **187**, 381 (2016).
2. M. Roca-Ayats, E. Herreros, G. García, M. A. Pena and M. V. Martínez-Huerta, *Appl. Catal. B: Environ.*, **183**, 53 (2016).
3. D. Chen and S. D. Minteer, *J. Power Sources*, **284**, 27 (2015).
4. Y. Liang, Q. Liu, A. M. Asiri, X. Sun and Y. He, *Int. J. Hydrogen Energy*, **40**, 13258 (2015).
5. B. B. Zhang, J. C. Xu, P. F. Wang, Y. B. Han, B. Hong, H. X. Jin, D. F. Jin, X. L. Peng, J. Li, J. Gong, H. L. Ge, Z. W. Zhu and X. Q. Wang, *J. Alloys Compd.*, **662**, 348 (2016).
6. M. Gong, Y. G. Li, H. L. Wang, Y. Y. Liang, J. Z. Wu, J. G. Zhou, J. Wang, T. Regier, F. Wei and H. J. Dai, *J. Am. Chem. Soc.*, **135**, 8452 (2013).
7. K. Akihiko and M. Yugo, *Chem. Soc. Rev.*, **38**, 253 (2009).
8. F. Y. Cheng and J. Chen, *Chem. Soc. Rev.*, **41**, 2172 (2012).
9. Y. C. Lu, Z. C. Xu, H. A. Gasteiger, S. L. Chen, K. Hamad-Schifferli and Y. Shao-Horn, *J. Am. Chem. Soc.*, **132**, 12170 (2010).
10. M. E. G. Lyons and M. P. Brandon, *J. Electroanal. Chem.*, **641**, 119(2010).
11. Y. Zhang, X. Cao, H. Yuan, W. Zhang and Z. Zhou, *Int. J. Hydrogen Energy*, **24**, 529 (1999).

12. W. J. King and A. C. Tseung, *Electrochim. Acta*, **19**, 493 (1974).
13. J. Haenen, W. Visscher and E. Barendrecht, *J. Electroanal. Chem*., **208**, 297 (1986).
14. Y. M. Lee, J. Suntivich, K. J. May, E. E. Perry and Y. Shao-Horn, *J. Phys. Chem. Lett*., **3**, 399 (2012).
15. W. H. Lee and H. Kim, *Catal. Comm*., **12**, 408 (2011).
16. W. Hu, Y. Q. Wang, X. H. Hu, Y. Q. Zhou and S. L. Chen, *J. Mater. Chem*., **22**, 6010 (2012).
17. J. Suntivich, K. J. May, H. A. Gasteiger, J. B. Goodenough and S. H. Yang, *Science*, **334**, 1383 (2011).
18. C. Jin, X. Cao, L. Zhang, C. Zhangand R. Yang, *J. Power Sources*, **241**, 225 (2013).
19. M. R. Gao, Y. F. Xu, J. Jiang, Y. R. Zheng and S. H. Yu, *J. Am. Chem. Soc*., **134**, 2930 (2012).
20. D. K. Bediako, B. Lassalle-Kaiser, Y. Surendranath, J. Yano, V. K. Yachandra and D. G. Nocera, *J. Am. Chem. Soc*., **134**, 6801 (2012).
21. K. Kadakia, M. K. Datta, P. H. Jampani, S. K. Park and P. N. Kumta, *J. Power Sources*, **222**, 313 (2013).
22. B. G. Lu, D. X. Cao, P. Wang, G. L. Wang and Y. Y. Gao, *Int. J. Hydrogen Energy*, **36**, 72(2011).
23. W. Bian, Z. Yang, P. Strasser and R. Yang, *J. Power Sources*, **250**, 196 (2014).
24. B. Kumar, S. Saha, K. Ojha and A. K. Ganguli, *Mater. Res. Bull*., **64**, 283 (2015).
25. A. S. Danial, M. M. Saleh, S. A. Salih and M. I. Awad, *J. Power Sources*, **293**, 101 (2015).
26. A. M. Ghonim, B. E. El-Anadouli and M. M. Saleh, *Electrochim. Acta*, **114**, 713 (2013).
27. R. H. Tammam, A. M. Fekry and M. M. Saleh, *Int. J. Hydrogen Energy*, **40**, 275 (2015).
28. R. M. A. Hameed and R. M. El-Sherif, *Appl. Catal. B: Environ*., **162**, 217 (2015).
29. M. Görlin, M. Gliech, J. F. de Araújo, S. Dresp, A. Bergmann and P. Strasser, *Catal. Today*, **262**, 65 (2016).
30. S. Yoon, J.-Y. Yun, J.-H. Lim and B. Yoo, *J. Alloys Compd*., **693**, 964 (2017).
31. B. P. Lu, B. Jing, X. J. Bo, L. D. Zhu and L. P. Guo, *Electrochim. Acta*, **55**, 8724 (2010).
32. D. A. Corrigan, *J. Electrochem. Soc*., **134**, 377 (1987).
33. F. Dionigi and P. Strasser, *Adv. Energy Mater*., **6**, 1600621 (2016).
34. J. R. Galán-Mascarós, *Chem. Electrochem*., **2**, 37 (2015).
35. I. Roger and M. D. Symes, *J. Mater. Chem*., **4**, 6724 (2016).
36. I. Roger, M. A. Shipman and M. D. Symes, *Nat. Rev. Chem*., **1**, 0003 (2017).
37. S. Klaus, Y. Cai, M. W. Louie, L. Trotochaud and A. T. Bell, *J. Phys. Chem. C*, **119**, 7243 (2015).
38. A. B. Moghaddam, M. R. Ganjali, R. Dinarvand, T. Razavi, A. A. Saboury, A. A. M.-Movahedi and P. Norouz, *J. Electroanal. Chem*., **614**, 83 (2008).
39. S. M. El-Refaei, M. M. Saleh and M. I. Awad, *J. Power Sources*, **223**, 125 (2013).
40. E. Laouini, Y. Berghoute, J. Douch, H. Mendonca, M. Hamdani and M. I. S. Pereira, *J. Appl. Electrochem*., **39**, 2469 (2009).
41. Z. Ding, C. Yang and Q. Wu, *Electrochim. Acta*, **49**, 3155 (2004).
42. M. Kumar, R. Awasthi, A. S. K. Sinh and R. N. Singh, *Int. J. Hydrogen Energy*, **36**, 8831 (2011).
43. M. Isabel Godinho, M. Alice Catarino, M. I. da Silva Pereira, M. H. Mendonca and F. M. Costa, *Electrochim. Acta*, **47**, 4307 (2002).
44. M. H. Mendonça, M. I. Godinho, M. A. Catarino, M. I. da Silva Pereira and F. M. Costa, *Solid State Sci*., **4**, 175 (2002).
45. N. Jiang and H.-m. Meng, *Surf. Coat. Technol*., **206**, 4362 (2012).
46. F. Rosalbino, S. Delsante, G. Borzone and G. Scavino, *Int. J. Hydrogen Energy*, **38**, 10170 (2013).
47. S. M. El-Refaei, M. M. Saleh and M. I. Awad, *J. Solid-State Electrochem*., **18**, 5 (2014).
48. S. M. El-Refaei, M. I. Awad, B. E. El-Anadouli and M. M. Saleh, *Electrochim. Acta*, **92**, 460 (2013).
49. J. M. Gonçalves, T. A. Matias, L. P. Saravia, M. Nakamura, J. S. Bernardes, M. Bertotti and K. Araki, *Electrochim. Acta*, **267**, 161 (2018).
50. L. Trotochaud, S. L. Young, J. K. Ranney and S. W. Boettcher. *J. Am. Chem. Soc*., **136**, 6744 (2014).
51. Q. Liu, H. Wang, X. Wang, R. Tong, X. Zhou, X. Peng, H. Wang, H. Tao and Z. Zhang. *Int J. Hydrogen Energy*, **42**, 5560 (2017).
52. Q. Luo, M. Peng, X. Sun, Y. Luo and A. M. Asiri, *Int. J. Hydrogen Energy*, **41**, 8785 (2016).
53. X. Yang, J. Pan, Y. Nie, Y. Sun and P. Wan, *Int. J. Hydrogen Energy*, **42**, 26575 (2017).
54. C. Zhang, Y. Xie, H. Deng, C. Zhang, J. W. Su, Y. Dong and J. Lin, *Int. J. Hydrogen Energy*, **43**, 7299 (2018).
55. H. B. Hassan and R. H. Tammam, *Solid State Ionics*, **320**, 325 (2018).
56. R. H. Tammam and H. B. Hassan, *J. Electrochem. Soc*., **166**, F729 (2019).
57. D. D. Macdonald, *Electrochim. Acta*, **51**, 1376 (2006).
58. A. M. Fekry and R. H. Tammam, *Ind. Eng. Chem. Res. J*., **53**, 2911 (2014).
59. R. H. Tammam and A. M. Fekry, *J. Mater. Eng. Perform*., **23**, 715 (2014).
60. E. Gombos, K. Barkács, T. Felföldi, C.Vértes, M. Makó, G. Palkó and G. Záray, *Microchem. J*., **107**, 115 (2013).
61. V. K. Sharma, *Coord. Chem. Rev*., **257**, 495 (2013).
62. J. Kubisztal and A. Budniok, *Int. J. Hydrogen Energy*, **33**, 4488 (2008).
63. D. Cibrev, M. Jankulovska, T. Lana-Villarreal and R. Gómez, *Int. J. Hydrogen Energy*, **38**, 2746 (2013).
64. M. F. Kibria and M. S. Mridha, *Int. J. Hydrogen Energy*, **21**, 179 (1996).
65. R. H. Tammam and M. M. Saleh, *J. Electroanal. Chem*., **794**, 189 (2017).

Supporting Information

Enhanced oxygen evolution reaction over glassy carbon electrode modified with NiO_x and Fe_3O_4

Reham Helmy Tammam†, Amany Mohamed Fekry, and Mahmoud Mohamed Saleh

Chemistry Department, Faculty of Science, Cairo University, Giza, Egypt
(*Received 7 March 2019 • accepted 2 September 2019*)

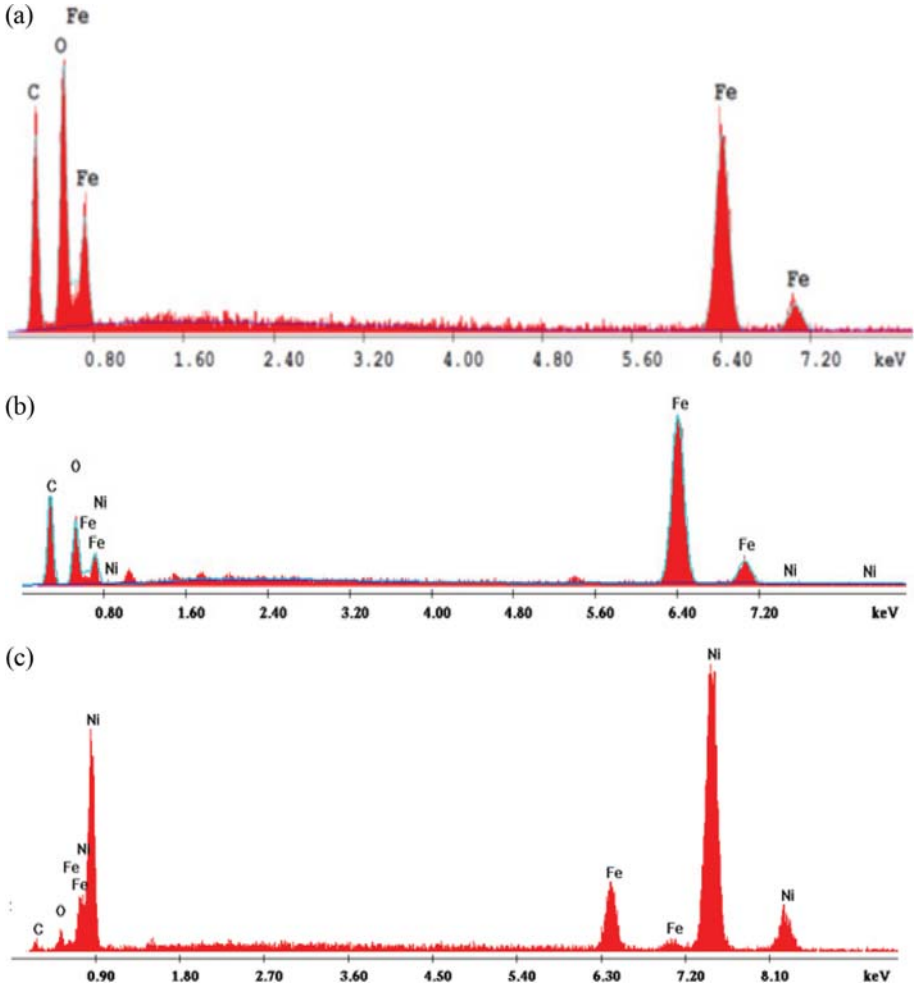

Fig. S1. EDX for GC/Fe_3O_4 (a), GC/NiO_x/Fe_3O_4 (b) and GC/Fe_3O_4/NiO_x (c).

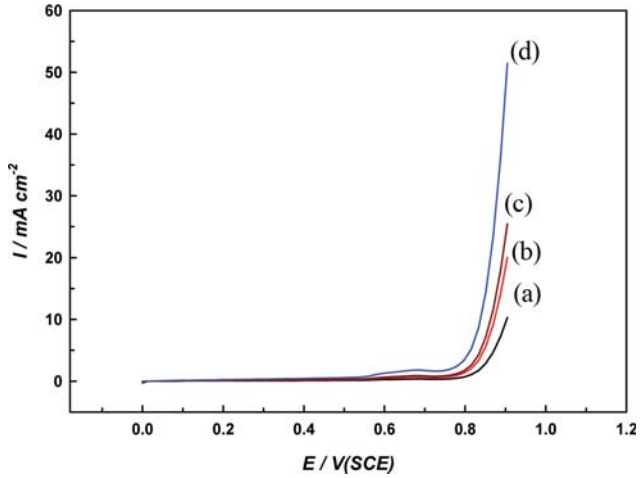

Fig. S2. LSV for OER in 0.5 M NaOH on GC/NiO_x of different loadings of NiO_x: (a) 0.029, (b) 0.075, (c) 0.240 and (d) 0.529 mg cm^{-2}, at a scan rate of 10 mV s^{-1}.